# Physical simulation of perovskite/ silicon three-terminal tandems based on bipolar transistor structure

Giliberti, Gemma, Cappelluti, Federica

Gemma Giliberti, Federica Cappelluti, "Physical simulation of perovskite/ silicon three-terminal tandems based on bipolar transistor structure," Proc. SPIE 11996, Physics, Simulation, and Photonic Engineering of Photovoltaic Devices XI, 1199602 (4 March 2022); doi: 10.1117/12.2609510

SPIE.

Event: SPIE OPTO, 2022, San Francisco, California, United States

# Physical Simulation of Perovskite/Silicon Three-Terminal Tandems Based on Bipolar Transistor Structure

Gemma Giliberti[a] and Federica Cappelluti[a]

[a]Dipartimento di Elettronica e Telecomunicazioni, Politecnico di Torino, Corso Duca degli Abruzzi 24, 10129, Torino (TO), Italia

## ABSTRACT

Tandem solar cells made of organometal halide perovskite and crystalline silicon cells are one of the most promising routes towards high efficiency low cost photovoltaics. Among the possible architectures, monolithic three-terminal tandems hold the promise of the highest energy/cost figure of merit, by combining the advantage of two- and four-terminal approaches. Recently, three-terminal perovskite/silicon tandems have been reported, based on interdigitated back contact heterojunction silicon cells. Alternative solutions that can be integrated with double-sided contact silicon cells are worth to be investigated in view of their higher compatibility with industrial mass production. In this work, we present a simulation-based proof-of-concept of PVK/Si three-terminal tandem cells that use a heterostructure bipolar transistor structure. The extra terminal is implemented at the common selective layer between the perovskite and silicon subcells, avoiding the use of any recombination layer or tunneling junction. We demonstrate promising device performance through physics-based simulations preliminarily validated against experimental data of other perovskite/silicon tandem technologies reported in literature.

**Keywords:** perovskite; silicon tandem; multijunction architecture; heterostructure bipolar transistor; textured solar cell; HIT solar cell; three-terminal; double junction.

## 1. INTRODUCTION

Organometal halide perovskites are among the most promising candidates as top sub-cell for silicon based tandems because of their excellent electrical and optical properties and low-cost technology. In monolithic two-terminal (2T) tandems, the perovskite (PVK) solar cell stack is directly deposited on top of the silicon bottom cell, either with flat or textured surface,[1,2] and the two sub-cells are electrically connected through a tunnel junction or recombination layer. For maximum power conversion efficiency, the series connection demands that the two subcells generate high and similar currents, making the solar cell performance sensitive to spectral variations and limiting the attainable real world energy yield.

To overcome the current matching constraint while retaining a monolithic structure, a viable alternative is offered by the three terminal (3T) architecture, which features a third contact allowing for independent power extraction from the two subcells.[3,4] PVK/Si 3T tandem have been reported where the third terminal is implemented at the recombination layer connecting the two subcells,[5] or at the rear side of the silicon cell adopting an interdigitated back contact design.[6] Besides these approaches, the novel multijunction architecture based on the heterojunction bipolar transistor (3T-HBT) structure[7,8] appears as a promising, yet rather unexplored, route towards 3T monolithic PVK/Si tandems compatible with both heterojunction and homojunction c-Si cells. In the 3T-HBT solar cell, one common layer (base) is shared between the top and bottom subcells' stack and used to realize an electrical contact for one type of carriers (e.g. holes), while the other type of carrier (e.g. electrons) is collected at the other two terminals (emitter and collector), one for each subcell. This allows for the independent operation of the two sub-cells without the use of any recombination layer, minimizing parasitic optical losses and carrier loss in case of electrical shunts.

Further author information:
Gemma Giliberti: E-mail: gemma.giliberti@polito.it
Federica Cappelluti: E-mail: federica.cappelluti@polito.it

Physics, Simulation, and Photonic Engineering of Photovoltaic Devices XI, edited by Alexandre Freundlich, Stéphane Collin, Karin Hinzer, Proc. of SPIE Vol. 11996, 1199602 · © 2022 SPIE · 0277-786X · doi: 10.1117/12.2609510

In this work, we present a preliminary design of a PVK/Si 3T-HBT tandem using a c-Si heterojunction bottom cell and investigate its performance with physics-based simulations encompassing optical and transport aspects. The 3T-HBT tandem is developed starting from the fully textured monolithic perovskite/silicon 2T tandem solar cell reported by Sahli et al.[9] Simulations are firstly verified against the experimental data in[9] and then used to analyze the performance of the proposed PVK/Si 3T-HBT solar cell with respect to that one of the 2T tandem.

## 2. MODEL & EXPERIMENTAL VALIDATION

We take as reference the fully textured PVK/silicon tandem[9] shown in Fig. 1. It consists of a PVK top cell and a silicon bottom cell with heterojunction with intrinsic thin-layer (HIT) on both sides, interconnected through a $p^{++}/n^{++}$ nc-Si tunnel junction. The conformal deposition of textured perovskite layers leads not only to a high compatibility with industrial silicon cells with front/rear textures, but also to improved light management.[1,9] From the top, the 100 nm thick $MgF_2$ layer is the anti-reflection coating layer, and the 110 nm thick indium zinc oxide (IZO) layer acts as transparent front electrode.[9] The PVK subcell consists of: 10 nm $SnO_2$ layer,[10,11] 15 nm $C_{60}$[12] electron selective layer, 440 nm of photo-absorbing mixed perovskite layer[13–15] and 12 nm thick Spiro-TTB hole transport layer.[10,14] The HIT subcell consists of 260 $\mu$m $n$-doped c-Si ($N_D = 2 \times 10^{15}$ cm$^{-3}$)[16] sandwiched by two thin-films of hydrogenated amorphous silicon: from the top (bottom) 5 (11) nm of $n$- ($p$-) doped a-Si:H[16] and 6 nm of intrinsic a-Si:H. The bottom cell is capped on its rear side by a 70 nm thick indium tin oxide (ITO) layer.

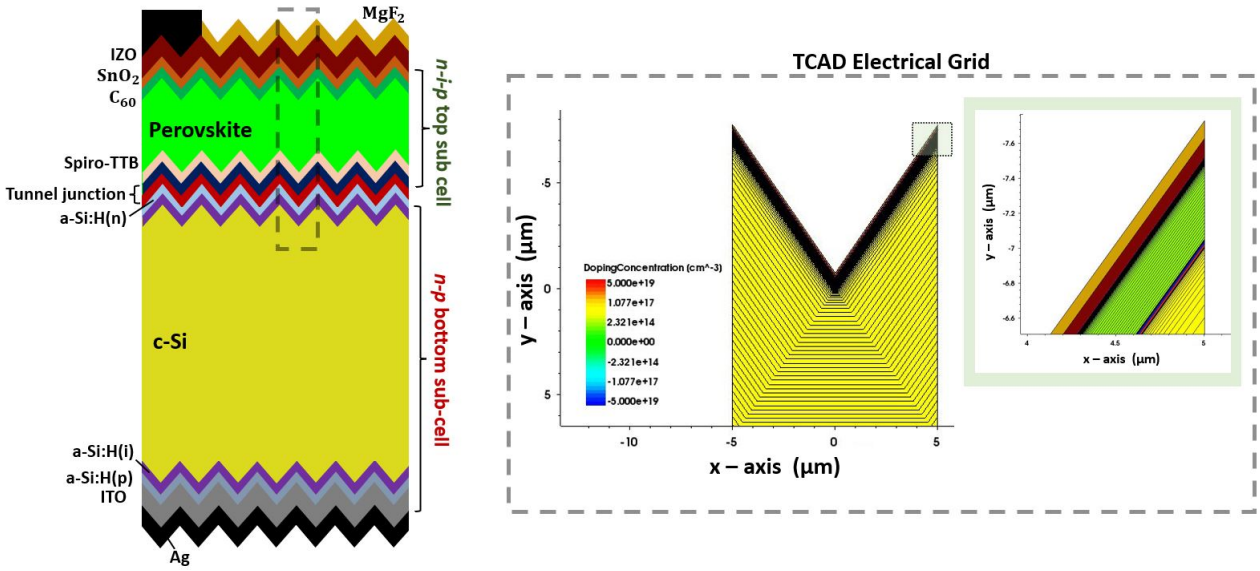


Figure 1. Schematic view of the simulated fully textured PVK/HIT-silicon tandem solar cell. In the dashed box, a zoom of the unit cell defining the TCAD simulation grid.

The opto-electronic model is developed within Sentaurus Technology Computer-Aided Design (TCAD) software from Synopsys.[17] For the textured surfaces, we assume a regular inverted pyramidal texture with silicon characteristic base angle of 54.7° and height of 7$\mu$m.[16] Taking advantage of the assumed periodicity, optical simulations are done on the smallest symmetry element of the structure, i.e. a single pyramid unit. We assume normal incidence and an input optical power of 100mW/cm$^2$ (AM1.5G spectrum). Optical simulations are carried out using a hybrid optical model, which combines transfer matrix method (TMM) and Monte Carlo RayTracing to asses both interference effects through the subwavelength multilayered media and scattering effects at the textured surfaces. In more detail, the angle at which the ray is incident on the first layer of the textured surface is passed as input to the TMM solver, which simulates the incidence-angle-dependent propagation across the thin film layers; the resulting optical characteristics, i.e. reflectance, transmittance and absorbance for the two

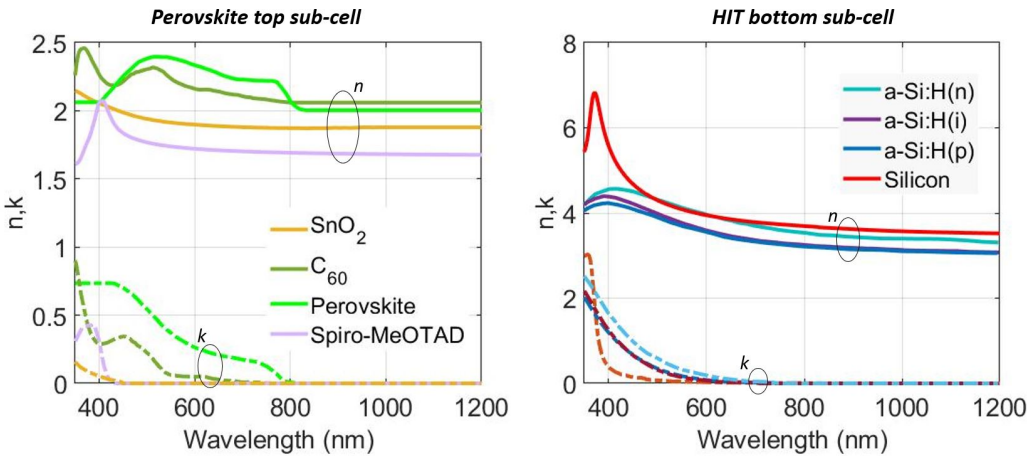


Figure 2. Refractive index ($n$ - solid line) and extinction coefficient ($k$ - dashed line) of the materials forming the PVK and HIT sub-cells.

polarizations, are used to set the boundary condition for the raytracer at the front and rear interface of the c-Si substrate. As a result, the simulation provides the 2D (or 3D) map of the optical generation rate across the device, included the absorbing thin films simulated by TMM. The obtained photogeneration rate distribution is then averaged to define a 1D profile given as input to the classical Poisson-drift-diffusion (DD) transport model.

Fig. 2 reports the wavelength-dependent complex refractive index for the optical simulation, while the main material parameters for the electrical simulation are summarized in Table 1. The perovskite material is modeled as a classical inorganic semiconductor, in agreement with previous works in literature.[14,18,19] As for recombination mechanisms, the model includes Shockely-Read-Hall recombination in the c-Si substrate only, with e/h time constants of 1 ms; Auger coefficients in silicon are modeled following.[20] Finally, the radiative recombination coefficient is set to: $1.8 \times 10^{-15}$ cm$^3$/s for a-Si:H, $4.73 \times 10^{-15}$ cm$^3$/s for c-Si, and $8 \times 10^{-10}$ cm$^3$/s for all the materials of the PVK subcell.

Fig. 3 compares the simulated External Quantum Efficiency (EQE) spectrum and the current-voltage ($J-V$) characteristics of the PVK/HIT-silicon tandem with the experimental ones reported in,[9] showing good agreement. The presented simulations have been done in 2D, simulating in fact a triangular texture. This might be the main reason for the slightly lower calculated EQE of the HIT-silicon sub-cell with respect to the measured one. On the other hand, the mismatch in the PVK wavelength range could be attributed to some inaccuracy in the assumed geometrical features and to some uncertainty in the material parameters, such as the extintion coefficient of the perovskite material which is heavily dependent on the composition of the perovskite.[22] The calculated

| | **PVK Top cell** | | | **HIT Bottom cell** | | | |
|---|---|---|---|---|---|---|---|
| | **Spiro-TTB** | **Perovskite** | **$SnO_2$** | **$C_{60}$**[21] | **a-Si:H(n/p)**[16] | **a-Si:H(i)**[16] | **c-Si**[17] |
| $E_g$ [eV] | 2.95[10] | 1.54[10] | 3.28[10] | 1.7 | 1.7 | 1.7 | 1.1 |
| $q\chi$ [eV] | 2.18 | 3.93 | 4.35 | 4.2 | 3.9 | 3.9 | 4.05 |
| $\epsilon_r$ | 3 | 6.5[15] | 9.6 | 4.1 | 11.9 | 11.9 | 11.9 |
| $N_c$ [cm$^{-3}$] | $2.2 \times 10^{18}$ | $2 \times 10^{18}$ | $4.1 \times 10^{18}$ | $1.44 \times 10^{21}$ | $2.5 \times 10^{20}$ | $2.5 \times 10^{20}$ | $2.9 \times 10^{19}$ |
| $N_v$ [cm$^{-3}$] | $1.8 \times 10^{19}$ | $2 \times 10^{18}$ | $4.1 \times 10^{18}$ | $1.44 \times 10^{21}$ | $2.5 \times 10^{20}$ | $2.5 \times 10^{20}$ | $1.8 \times 10^{19}$ |
| $\mu^{[e]}$ [cm$^2$/Vs] | 0.0002[14] | 11.8[14] | 240[11] | 1.6 | 5 | 20 | 1417 |
| $\mu^{[h]}$ [cm$^2$/Vs] | 0.0002[14] | 11.8[14] | 240[11] | 1.6 | 1 | 5 | 470 |
| $N$ [cm$^{-3}$] | $-5 \times 10^{18}$ | $2 \times 10^{14}$ | $5 \times 10^{18}$ | $5 \times 10^{18}$ | $10^{19}/-10^{19}$ | $10^{14}$ | $2 \times 10^{15}$ |

Table 1. Main material parameters. $E_g$: bandgap; $\chi$: electron affinity; $\epsilon_r$: relative permittivity; $N_c(N_v)$: effective density of states in conduction (valence) band; $\mu$: mobility; $N$: net doping; [e/h]: electron/hole; if not specified, the value shown applies to both carriers.

short circuit current density ($J_{sc}$) for PVK and HIT-silicon subcell results as 21.1 and 18.5 $\mathtt{mA/cm^2}$, respectively, against the measured ones of 20.1 and 20.3 $\mathtt{mA/cm^2}$. The calculated open circuit voltage ($V_{oc}$) of the standalone PVK and HIT cells results as $\sim 1.04\mathtt{V}$ and $\sim 0.71\mathtt{V}$, respectively, well matched to the experimental values. The tandem cell reaches a total $V_{oc}$ of $\approx 1.75$ V, about 30 mV lower than the measured one, yielding an estimated tandem efficiency of 28.1 %. From the comparison in Fig. 3, it is apparent that the simulated fill factor (FF) is significantly higher than the measured one. This stems from the fact that the model neglects any enhanced recombination at the textured surfaces as well as defect assisted recombination in the thin film layers.

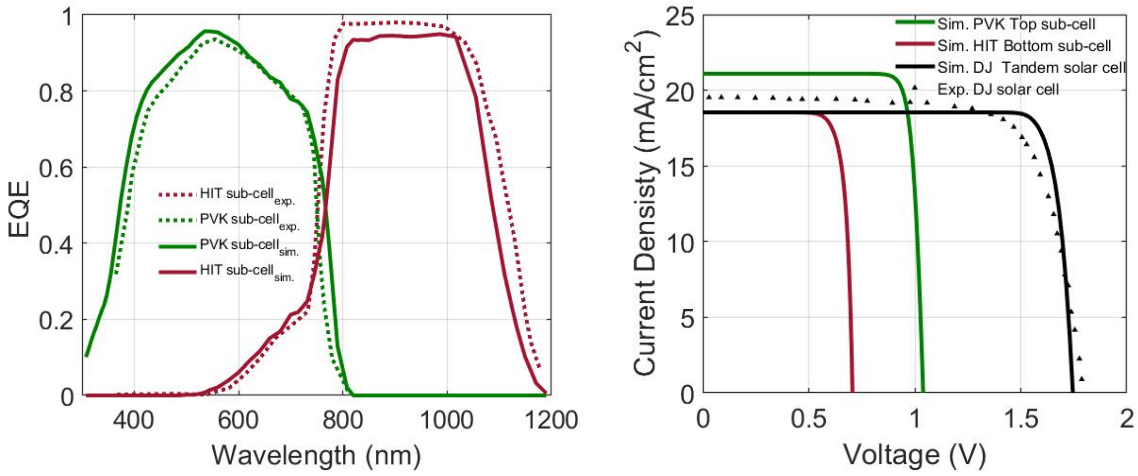


Figure 3. Comparison between simulated (solid lines) and measured (dashed lines) EQE and $J-V$ characteristics of the fully-textured 2T PVK/Si tandem in.[9]

## 3. PERFORMANCE OF THE PEROVSKITE/SILICON 3T-HBT SOLAR CELL

The PVK/Silicon 3T-HBT solar cell is developed based on the *n-p-n* structure of a bipolar junction transistor, whose regions are named as emitter, base and collector. The multilayer stack of our proposed PVK/HIT 3T-HBT tandem is sketched in Fig. 4. It consists of two sub-cells, i.e. the *n-i-p* emitter-base (EB) and the *p-n* base-collector (BC), that are electrically connected through the common base layer. In particular, the $SnO_2$, $C_{60}$, and PVK layers form the *n*-doped emitter region, the Spiro-TTB and (p)-(i) a-Si:H layers form the *p*-doped base region and finally the c-Si and (i)-(n) a-Si:H layers form the *n*-doped collector region. Compared to the 2T double junction (DJ) solar cell studied in the previous section, the 3T-HBT tandem is obtained by removing the tunnel junction, flipping the *n-p* HIT that is now illuminated from the *p* side, and implementing the third contact at the base region. The lateral base contact is implemented at the Spiro-TTB layer.

While the DJ architecture is characterized by two sub-cells interconnected in series and only one external load, in the 3T-HBTsc we can detect two back-to-back PVK/HIT sub-cells whose generated electrical power is extracted at two independent loads, relaxing the current matching constraint. The multilayer stack is simpler than that one of the DJ tandem because the HBT architecture avoids the use of tunnel or recombination junction. However, the lateral base contact will require the development of ad hoc solutions able to minimize shadow loss and parastic resistances.[23]

The 3T-HBTsc of Fig.4 is simulated in Sentaurus TCAD with the same optical and electrical model described in Sec. 2. Fig.5 shows the simulated EQE and $J-V$ characteristic. The EQE of the HBT solar cell is almost identical to that one of the DJ tandem, because the high diffusion length of the HIT cell ensures a high collection efficiency regardless of the illuminated side, and the PVK cell is unchanged. If the PVK cell had been flipped, to obtain a *p-n-p* bipolar device, the optical response would be markedly different, due to the parasitic absorption of the hole transport layer and would have required a re-optimization of the design.[24] Concerning the photovoltaic performance, it is worth noticing that the high bandgap and doping of the *p*-doped Spiro-TTB and a-Si:H

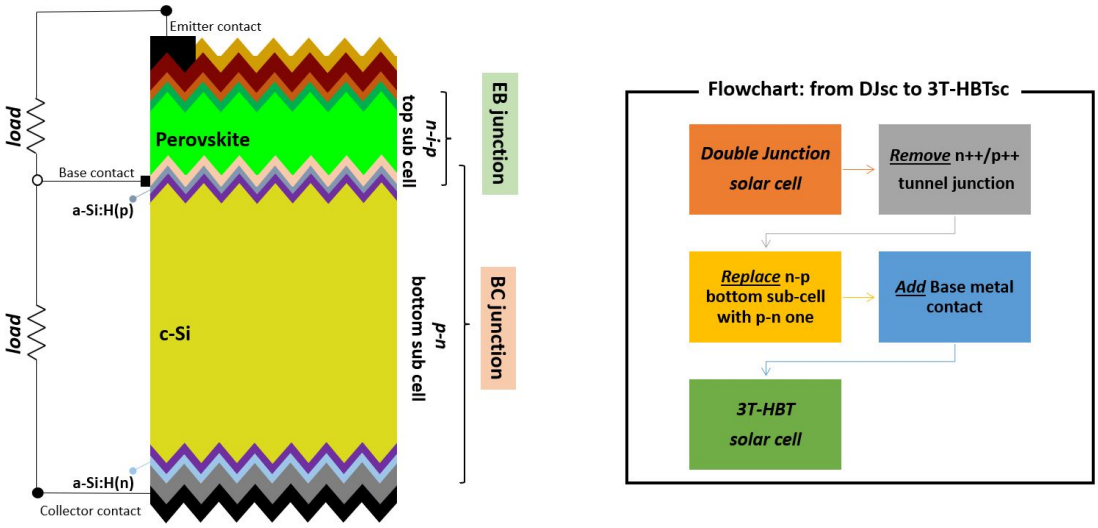


Figure 4. Schematic view of the proposed fully textured PVK/HIT-silicon 3T-HBT solar cell. In the box, a flowchart of the steps to turn the 2T tandem into a 3T-HBT tandem.

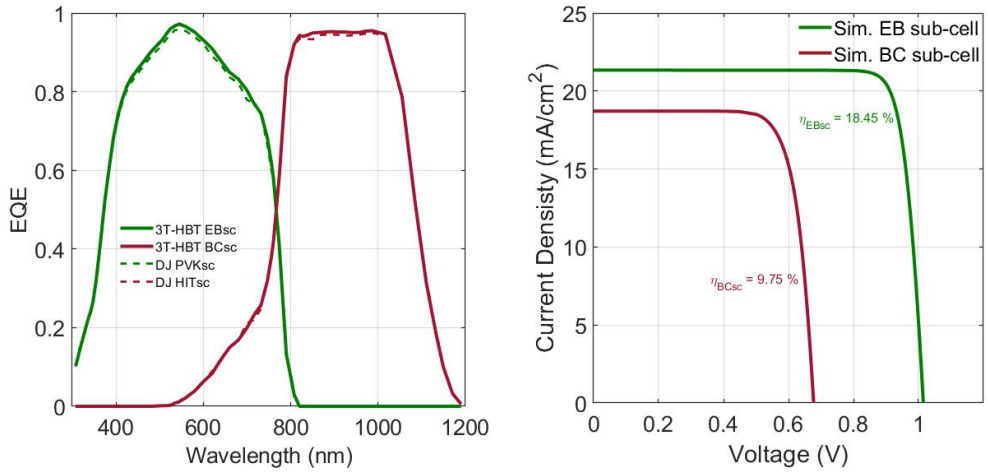


Figure 5. Simulated EQE and $J-V$ characteristics of the 3T-HBT tandem. For reference, the EQE spectra are compared to those of a DJ tandem with the same geometry as in Fig. 1 but with $n$-type c-Si.

layers prevent any cross-talk, or *transistor action*, between the emitter and collector region; this implies that the current-voltage characteristic of the bottom BC cell is invariant with respect to the bias condition of the top EB cell (at least up to the maximum power point) and conversely for the EB cell with respect to the operating voltage of the BC one.[7] Therefore, the individual $J-V$ characteristics shown in Fig. 5, are representative of the photovoltaic operation of the HBT tandem, which achieves a cumulative power conversion efficiency of $\sim 28.2\%$ with the two EB and BC sub-cells at maximum power point (0.89 V, 0.56 V), in line with that one of the baseline 2T tandem.

## 4. CONCLUSIONS

We have reported a preliminary simulation study of perovskite/silicon three-terminal tandem solar cells based on the heterojunction bipolar transistor architecture. Results show that this novel architecture can realistically achieve the same performance of the corresponding two terminal tandem with the advantage of a simpler multilayer stack, since no tunnel junction or recombination layer are needed. The bipolar transistor architecture is

suitable for the development of perovskite/silicon cells compatible with heterojunction and homojunction c-Si technologies which hold about 90% of the photovoltaic market. The promising performance of the intrinsic device prompt for further studies to devise novel grid architectures able to minimize shadow and resistive loss connected with the implementation of the extra base terminal.

## REFERENCES


[1] Jäger, K., Sutter, J., Hammerschmidt, M., Schneider, P.-I., and Becker, C., "Prospects of light management in perovskite/silicon tandem solar cells," *Nanophotonics* **10**(8), 1991–2000 (2020).

[2] Lehr, J., Langenhorst, M., Schmager, R., Kirner, S., Lemmer, U., Richards, B. S., Case, C., and Paetzold, U. W., "Energy yield modelling of perovskite/silicon two-terminal tandem pv modules with flat and textured interfaces," *Sustainable Energy & Fuels* **2**(12), 2754–2761 (2018).

[3] Warren, E. L., Deceglie, M. G., Rienäcker, M., Peibst, R., Tamboli, A. C., and Stradins, P., "Maximizing tandem solar cell power extraction using a three-terminal design," *Sustainable Energy & Fuels* **2**(6), 1141–1147 (2018).

[4] Gota, F., Langenhorst, M., Schmager, R., Lehr, J., and Paetzold, U. W., "Energy yield advantages of three-terminal perovskite-silicon tandem photovoltaics," *Joule* **4**(11), 2387–2403 (2020).

[5] Park, I. J., Park, J. H., Ji, S. G., Park, M.-A., Jang, J. H., and Kim, J. Y., "A three-terminal monolithic perovskite/si tandem solar cell characterization platform," *Joule* **3**(3), 807–818 (2019).

[6] Tockhorn, P., Wagner, P., Kegelmann, L., Stang, J.-C., Mews, M., Albrecht, S., and Korte, L., "Three-terminal perovskite/silicon tandem solar cells with top and interdigitated rear contacts," *ACS Applied Energy Materials* **3**(2), 1381–1392 (2020).

[7] Giliberti, G., Martí, A., and Cappelluti, F., "Perovskite-si solar cell: a three-terminal heterojunction bipolar transistor architecture," in [*2020 47th IEEE Photovoltaic Specialists Conference (PVSC)*], 2696–2699 (2020).

[8] Martí, A. and Luque, A., "Three-terminal heterojunction bipolar transistor solar cell for high-efficiency photovoltaic conversion," *Nature communications* **6**(1), 1–6 (2015).

[9] Sahli, F., Werner, J., Kamino, B. A., Bräuninger, M., Monnard, R., Paviet-Salomon, B., Barraud, L., Ding, L., Diaz Leon, J. J., Sacchetto, D., Cattaneo, G., Despeisse, M., Boccard, M., Nicolay, S., Jeangros, Q., Niesen, B., and Ballif, C., "Fully textured monolithic perovskite/silicon tandem solar cells with 25.2% power conversion efficiency," *Nature materials* **17**(9), 820–826 (2018).

[10] Jošt, M., Kegelmann, L., Korte, L., and Albrecht, S., "Monolithic perovskite tandem solar cells: A review of the present status and advanced characterization methods toward 30% efficiency," *Advanced energy materials* **10**(26), 1904102–n/a (2020).

[11] Chen, Y., Meng, Q., Zhang, L., Han, C., Gao, H., Zhang, Y., and Yan, H., "Sno2-based electron transporting layer materials for perovskite solar cells: A review of recent progress," *Journal of energy chemistry* **35**, 144–167 (2019).

[12] Stübinger, T., "Optische modellierung und charakterisierung von organischen donor-akzeptor solarzellen," (2005).

[13] Correa-Baena, J.-P., Anaya, M., Lozano, G., Tress, W., Domanski, K., Saliba, M., Matsui, T., Jacobsson, T. J., Calvo, M. E., Abate, A., Grätzel, M., Míguez, H., and Hagfeldt, A., "Unbroken perovskite: Interplay of morphology, electro-optical properties, and ionic movement," *Advanced Materials* **28**(25), 5031–5037 (2016).

[14] Olyaeefar, B., Ahmadi-Kandjani, S., and Asgari, A., "Bulk and interface recombination in planar lead halide perovskite solar cells: A drift-diffusion study," *Physica E: Low-dimensional Systems and Nanostructures* **94**, 118–122 (2017).

[15] Imran, H., Durrani, I., Kamran, M., Abdolkader, T. M., Faryad, M., and Butt, N. Z., "High-performance bifacial perovskite/silicon double-tandem solar cell," *IEEE journal of photovoltaics* **8**(5), 1222–1229 (2018).

[16] Tonita, E. M., Valdivia, C. E., Martinez-Szewczyk, M., Lewis, M. R., Bertoni, M. I., and Hinzer, K., "Effect of air mass on carrier losses in bifacial silicon heterojunction solar cells," *Solar Energy Materials and Solar Cells* **230**, 111293 (2021).

[17] "Sentaurus Device, Synopsys Inc.," (2017).

[18] Alnuaimi, A., Almansouri, I., and Nayfeh, A., "Effect of mobility and band structure of hole transport layer in planar heterojunction perovskite solar cells using 2d tcad simulation," *Journal of computational electronics* **15**(3), 1110–1118 (2016).

[19] Miyano, K., Tripathi, N., Yanagida, M., and Shirai, Y., "Lead halide perovskite photovoltaic as a model p–i–n diode," *Accounts of chemical research* **49**(2), 303–310 (2016).

[20] Häcker, R. and Hangleiter, A., "Intrinsic upper limits of the carrier lifetime in silicon," *Journal of Applied Physics* **75**(11), 7570–7572 (1994).

[21] Golubev, T., Liu, D., Lunt, R., and Duxbury, P., "Understanding the impact of c60 at the interface of perovskite solar cells via drift-diffusion modeling," *AIP Advances* **9**(3), 035026 (2019).

[22] Werner, J., Nogay, G., Sahli, F., Yang, T. C.-J., Bräuninger, M., Christmann, G., Walter, A., Kamino, B. A., Fiala, P., Löper, P., Nicolay, S., Jeangros, Q., Niesen, B., and Ballif, C., "Complex refractive indices of cesium–formamidinium-based mixed-halide perovskites with optical band gaps from 1.5 to 1.8 ev," *ACS Energy Letters* **3**(3), 742–747 (2018).

[23] Zehender, M., Svatek, S., Steiner, M., Garcia, I., Garcia-Linares, P., Warren, E., Tamboli, A., Martí, A., and Antolín, E., "Gainp/gaas three-terminal heterojunction bipolar transistor solar cell," *PREPRINT (Version 2) available at Research Square* (2021).

[24] Altazin, S., Stepanova, L., Werner, J., Niesen, B., Ballif, C., and Ruhstaller, B., "Design of perovskite/crystalline-silicon monolithic tandem solar cells," *Opt. Express* **26**, A579–A590 (May 2018).